

Pluto's atmospheric structure from the July 2007 stellar occultation



Catherine B. Olkin^{a,*}, Leslie A. Young^a, Richard G. French^b, Eliot F. Young^a, Marc W. Buie^a, Robert R. Howell^c, Jeffrey Regester^d, Catherine R. Ruhland^{a,1}, Tim Natusch^e, David J. Ramm^f

^a Southwest Research Institute, Department of Space Studies, 1050 Walnut St., Boulder, CO 80302, United States

^b 341A Green Hall, Wellesley College, Wellesley, MA 02481, United States

^c Department of Geology & Geophysics, University of Wyoming, 1000 E. University Dr., Laramie, WY 82071, United States

^d Greensboro Day School, 5401 Lawndale Dr., Greensboro, NC 27455, United States

^e Auckland University of Technology, University of Auckland, Auckland, New Zealand

^f Department of Physics and Astronomy, University of Canterbury, Christchurch, New Zealand

ARTICLE INFO

Article history:

Received 30 May 2011

Revised 11 May 2014

Accepted 13 May 2014

Available online 5 June 2014

Keywords:

Occultations

Pluto, atmosphere

Atmospheres, structure

ABSTRACT

In July 2007, we observed a stellar occultation by Pluto from three sites in New Zealand and Australia. From these occultation observations, we find that Pluto's atmospheric pressure is still at the increased level measured in 2002 and 2006 with a pressure at a radius of 1275 km of $2.09 \pm 0.09 \mu\text{bar}$. One of the sites, Mt. John Observatory, was ~ 70 km from the shadow center and we recorded the first central-flash occultation by Pluto. We carried out a dual-wavelength observation from this site with two different cameras using filtered high-time resolution observations in the visible from the one-meter telescope at Mt. John Observatory. From our central-flash observations, we find the elliptical shape that best matches the data corresponds to a nearly prolate atmosphere with an ellipticity of 0.09. The flux observed in the central-flash data can be fit equally well with either a haze layer or a thermal gradient in the altitudes probed by the occultation. However, the star light contributing to the central-flash occultation for the haze layer model would pass through a radius of 1130 km from Pluto's center. Given our current best estimate of Pluto's surface radius is greater than 1151 km (Tholen, D.J., Buie, M.W. [1997]. Bulk properties of Pluto and Charon. In: Stern, S.A., Tholen, D.J. (Eds.), Pluto and Charon. The University of Arizona Press), we prefer the thermal gradient solution or a combination of haze and thermal gradient to explain the occultation light curves.

© 2014 Elsevier Inc. All rights reserved.

1. Introduction

When methane ice was first detected on the surface of Pluto (Cruikshank et al., 1976), it was realized that Pluto could have an atmosphere supported by vapor–pressure equilibrium. The atmosphere was confirmed with the first published stellar occultation in 1988 (Elliot et al., 1989). In 1993, spectroscopic observations identified carbon monoxide and nitrogen ice on the surface of Pluto (Owen et al., 1993) in addition to methane ice. Because of the abundance of N_2 on the surface and its large vapor pressure compared to methane and carbon monoxide, it is expected that nitrogen is the dominant species in Pluto's atmosphere.

Pluto's atmosphere has also been directly detected. Young et al. (1997) were the first to observe a gaseous species in Pluto's atmosphere with their detection of methane from high-resolution

infrared spectroscopy. Recently CO has been detected in the radio and infrared (Greaves et al., 2011; Lellouch et al., 2011).

Despite attempts to observe stellar occultations by Pluto in the 1990s, it was not until 2002 that the next occultation was observed (Elliot et al., 2003; Sicardy et al., 2003). The 2002 event demonstrated that Pluto's atmospheric pressure had doubled in the 14 years between observations. Thermal models by Hansen and Paige (1996) had predicted possible large changes in atmospheric pressure due to varying insolation, but the models were not well constrained and these two occultations showed that Pluto's atmosphere does, in fact, vary dramatically. Subsequent occultation data have shown that the atmosphere has retained an atmospheric pressure near the measurement in 2002 (Young, 2013 and reference therein).

Opportunities for stellar occultation observations have been increasing in recent years, as Pluto has been passing in front of the galactic plane as seen from Earth. Because of the increased opportunities to probe Pluto's atmosphere with occultations and the changing insolation and aspect of Pluto, we initiated a program

* Corresponding author.

E-mail address: colkin@boulder.swri.edu (C.B. Olkin).

¹ Current address: Wheeler Trigg O'Donnell LLP, Denver, CO 80202, United States.

to monitor the seasonal change in Pluto's atmosphere as it recedes from the Sun (perihelion was in 1989). These observations also provide historical context for the close-up observations of Pluto that New Horizons will provide in 2015. As part of this program, we have successfully observed stellar occultations by Pluto every year from 2006 to 2014, sometimes with multiple occultation events per year (Young et al., 2008; Young, 2013). This paper presents results from the well-observed July 31, 2007 stellar occultation that was visible from Australia and New Zealand.

2. Observations

On July 31, 2007, Pluto passed in front of the star P495.3 (UCAC2 25815762; McDonald and Elliot, 2000) as seen from New Zealand and Australia. The star was relatively bright ($V = 13.2$) allowing for the use of smaller telescopes such as our 14-in. portable systems (Young et al., 2011) and allowing us to do a two-wavelength experiment at one of the larger aperture stations (Mt. John Observatory). The 1.0-m telescope at Mt. John Observatory was sufficiently large that we could use a dichroic to split the light (at a wavelength of 627 ± 20 nm) and still have sufficient SNR in the occultation light curves. The observed light curves had a SNR per scale height of 75 in the blue channel and 86 in the red channel. Another factor in selecting Mt. John for the dual wavelength observations was its high likelihood of being in the shadow path.

For the July 2007 occultation, observations were attempted from 7 locations; see Table 1 and Fig. 1. We used our PHOT cameras (Young et al., 2011) at 5 sites: (i) the Anglo-Australian Telescope (AAT), (ii) our portable telescope at Mussleroe Bay in northeast Tasmania, (iii) Mt. Canopus Observatory, (iv) Auckland Observatory, and (v) Mt. John Observatory. John Broughton recorded observations from Reedy Creek Observatory in Queensland, Australia and saw no occultation, consistent with our reconstructed geometry. Weather prohibited observations from Carter Observatory in Wellington, New Zealand and from the AAT which was outside the shadow path. Five occultation light curves were successfully

recorded from four sites: Mt. John (2 light curves), Mt. Canopus and Mussleroe Bay, and Auckland Observatory.

The purpose of the two-color experiment was used to characterize the amount of haze in Pluto's atmosphere. The residual flux in the central part of the Pluto occultation light curves from 1989 to the present is too low to be explained by a clear isothermal atmosphere alone. Instead either absorption by haze or refraction by a thermal inversion is required to explain the minimum stellar flux observed. If absorption by haze were responsible, then the minimum stellar flux would be a function of wavelength. If refraction from a thermal inversion layer caused the low stellar flux, then the observed light level would not change significantly with wavelength.

2.1. Mt. John Observatory

We built a mount for the 1-meter telescope at Mt. John that could accommodate two of our PHOT cameras (Young et al., 2011) and a 50-mm square dichroic plate of thickness 2 mm. The dichroic was purchased from Omega Optical and has a cut-on wavelength of 627 ± 20 nm, reflecting greater than 90% of the light from 400 to 600 nm and transmitting more than 85% of the light from 650 to 1100 nm. The effective wavelengths of these two observations are 0.51 and 0.76 μm .

The exposure times for both cameras at Mt. John Observatory were 0.25 s. The frame transfer cameras have essentially no dead-time. From this site, the topocentric shadow velocity was 16.8 km/s. The observations sample the scale height of Pluto's atmosphere (~ 60 km) well with a single exposure covering only 4.2 km. At $f/8$ and with a hardware binning of 2, the pixel scale was 0.84 arcsec/pixel.

For all datasets, the same photometric reduction was used. A combined bias-dark frame was subtracted from the data and then a normalized flat field was used to remove pixel-to-pixel variations. Aperture photometry with on-chip photometric standards was used for each of the data sets.

Table 1
Observing circumstances.

Site	Aperture (m)	Location (S lat., E long.)	Impact parameter (km) ^a	Exp. time/duty cycle (s)	S/N ^b	Effective wavelength (μm)	Observers	Weather
Mt. John	1.0	43°59'15" 170°27'54"	69 \pm 3	0.25/0.25	74 (B) 86 (R)	0.51 (B) 0.76 (R)	L. Young & Howell	Clear
Carter	0.4	41°17'03" 174°45'55"	–	–	–	–	Blow	Cloudy
Auckland ^c	0.4	36°54'28" 174°46'36"	484 \pm 3	1.0/1.0	<21 ^d	0.61	Natusch	Partially clear
Mt. Canopus	1.0	42°50'50" 147°25'58"	793 \pm 3	0.5/0.5	73	0.61	E. Young, Giles, Greenhill	Partially clear
Musselroe Bay	0.36	40°50'38" 148°10'45"	944 \pm 3	0.5/0.5	50	0.61	Register & Ruhland	Partially clear
AAT	4.0	31°16'37" 149°03'58"	–	–	–	–	Olkin & Shoemaker	Cloudy
Reedy Creek ^e	0.25	28°06'36" 153°23'49"	–	4.1/5.0	–	–	Broughton	Clear

^a The impact parameter is derived from the non-isothermal fit for the geometric solution (see Table 2). The impact parameter derived from the isothermal fit are 2 km less for each site than the values above.

^b The S/N is the signal-to-noise ratio in the unocculted signal over an interval during which Pluto's shadow moves 60 km.

^c The weather at Auckland Observatory was intermittently cloudy. We were unable to extract accurate photometry from the observations.

^d The SNR for the Auckland Observatory light curve is an upper limit because it is derived from the post-emersion baseline where the systematic effects from the weather are smaller.

^e Observations were obtained at Reedy Creek Observatory which is north of AAT and not in the shadow path.

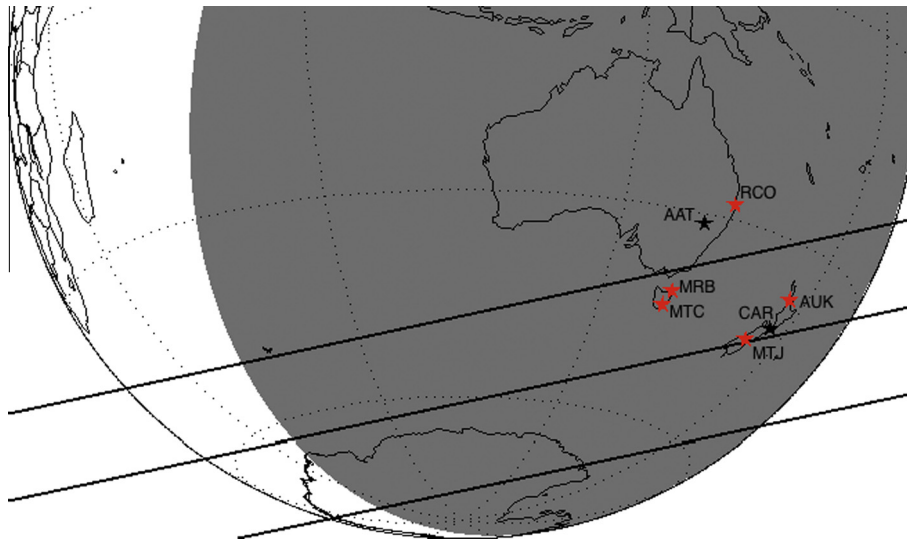


Fig. 1. The Earth as seen from Pluto at the occultation time. The lines (northern limit, centerline and southern limit) show the reconstructed occultation shadow path. The shaded region indicates where the Sun is below -12° altitude. We deployed occultation cameras to 5 sites. From north to south, these sites were Reedy Creek Observatory (RCO), the Anglo-Australian Telescope (AAT), Auckland Observatory (AUK), Musselroe Bay (MRB), Mt. Canopus Observatory (MTC), Carter Observatory (CAR) and Mt. John Observatory (MTJ). The red stars indicate sites that could observe during the predicted event time and the black stars indicate sites that were clouded out. (For interpretation of the references to color in this figure legend, the reader is referred to the web version of this article.)

2.2. Mt. Canopus Observatory

At Mt. Canopus Observatory, there were clouds on the night of the occultation. Fortunately, the clouds before the event were intermittent enough to allow the observers (Eliot Young, Barry Giles and John Greenhill) to get set up on the occultation star field. Clouds cleared in time for the event and then reemerged after the event. There were some lost frames due to clouds during the occultation, but not many, see Fig. 2. The data were recorded unfiltered, full-frame with a 0.5 s integration time and an on-chip binning factor of 2.

For the observations at all sites other than Mt. John, the observations were conducted with no filter. For the light curve data that was collected with our PHOT system (from the following sites: Mt. Canopus Observatory, Auckland Observatory and Musselroe Bay), the effective wavelength was $0.61 \mu\text{m}$ given the response of the detector as a function of wavelength.

2.3. Musselroe Bay

Our portable 14-in. Meade LX-200 telescope was enlisted for the occultation to provide a mobile station in case of bad weather. This was useful as most of Tasmania and southern Australia was covered in clouds the night of the occultation. The Musselroe Bay observers (Trina Ruhland and Jeff Regester) consulted with the New Zealand weather service to find a site with the highest probability of clear skies. The weather predictions were accurate and the observations were recorded under clear skies. To maximize SNR the observations were unfiltered. A subframe (256×256 pixels) of the whole detector was used to record the observations. A 15-min series of images was recorded with an exposure time of 0.5 s. There were some technical difficulties with the telescope tracking causing some gaps in the observations when the telescope pointing was adjusted. The loss of data due to tracking problems can be seen just after egress in Fig. 2. There were no tracking problems during the occultation itself. However, a few frames were lost due to clouds during the occultation.

Differential photometry was used to extract the occultation light curve from the data using an on-chip reference star. Unfortunately, observations of the occulted star when it was not blended

with Pluto–Charon were not recorded with the portable system at Musselroe Bay, Tasmania. However, both Mt. Canopus and Musselroe Bay observed unfiltered using the PHOT system allowing us to use the ratio of flux from Mt. Canopus to normalize the occultation light curve for both the Mt. Canopus and Musselroe Bay data. While there can be camera-to-camera variability in the response of the system, this is the best source of calibration that we have for the Musselroe Bay data.

2.4. Auckland Observatory

Observations were recorded from Auckland Observatory under difficult conditions including rain, clouds and only short periods of clear skies. Immersion was affected by clouds as can be seen by the large scatter in the data and difficulty in calibrating the normalized light curve. The immersion light curve should have a normalized flux near 1.0, but it is systematically high by more than 50% in some places due to the difficulty in removing the flux due to clouds from the signal. The Auckland site is in an urban area and streetlights combined with variable clouds make the accurate photometric calibration of these data impossible. Not only is the baseline data difficult to calibration, but also the central region of the light curve is also systematically affected by the clouds. Due to difficulties in photometric calibration of this light curve, we present the light curve here, but exclude it from the modeling.

The normalized stellar occultation light curves from all sites are given in Fig. 2 with their best fitting models (discussed in Section 3). All the data collected from these four sites used our PHOT camera systems.

3. Geometric solution and upper atmospheric modeling

A geometric solution and global atmospheric model was obtained by simultaneously fitting the 4 well-calibrated light curves using the Elliot and Young (1992) formulation, hereafter referred to as EY92. The fit assumed a circular half-light profile, i.e. the same half-light radius for all chords. We fit the 4 light curves simultaneously assuming a uniform atmosphere across all chords and allowing for a shift in the shadow location relative to the location predicted by the star position (RA: 17:45:41.9865;

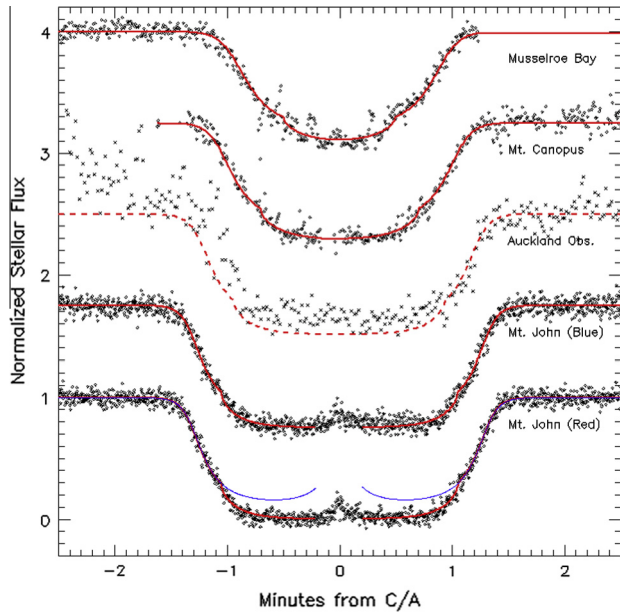


Fig. 2. The normalized occultation light curves with the best-fit isothermal model (red line) as a function of time from the closest approach (C/A) of the star to the planet. The occultation light curves are offset for clarity by 0.75 in normalized stellar flux. A clear isothermal atmosphere model (no haze) is shown in blue for the Mt. John (red filter) light curve to demonstrate that either a significant thermal gradient or haze below 1237 km from the center of Pluto is needed to match the data. The radius of 1237 km, corresponding to a normalized stellar flux level of 0.3, is where the red and blue curves diverge. In the light curve modeling for the geometric solution, we excluded the central-flash region of the Mt. John data where the model curve is not presented. The Auckland Observatory light curve is shown here for completeness, but it was not used in the solution and is therefore indicated with dashes. The Mt. Canopus Observatory light curve has a few data dropouts including before -1.5 min from closest approach, near the middle of the occultation and just after egress due to intermittent clouds. At Musselroe Bay tracking was lost due to technical issues post-emersion (near $+1.2$ min from closest approach), but it was regained soon after. The later (not displayed) baseline remained flat. (For interpretation of the references to color in this figure legend, the reader is referred to the web version of this article.)

Dec: $-16:29:31.690$, Equinox and Epoch J2000, UCAC2 position from Zacharias et al., 2004) and the Pluto ephemeris as defined by DE414 and Plu013. For the isothermal upper atmosphere, we assumed the light curves from each site had the same pressure, temperature and thermal gradient at a reference radius of 1275 km. For the lower atmosphere, we assumed the light curves from each site had the same haze onset radius, haze scale height and the linear absorption coefficient, see EY92. For each light curve, we used the effective wavelength and an assumption of a pure N_2 atmosphere to get the refractivity at STP. All the light curve data except the central-flash region of the Mt. John light curves and the Auckland Observatory light curve were used in the fit. For

Table 2
Model fits for geometric solution.

Parameter	Isothermal	Non-isothermal
f_0 (shadow shift in RA), km	499.9 ± 1.4	499.8 ± 1.3
g_0 (shadow shift in Dec), km	-845.0 ± 3.1	-843.1 ± 2.8
Temperature ^a , K	112.1 ± 1.5	103.2 ± 1.4
Pressure ^a , μ bar	2.38 ± 0.10	2.09 ± 0.09
dT/dr^a , K/km	0	-0.086
Radius at onset of haze, km	1236.7 ± 1.8	1236.7 ± 1.6
Scale height of haze, km	2.01 ± 0.11	1.97 ± 0.11
Haze linear absorption coefficient, 1000/km	40.7 ± 3.9	41.1 ± 3.5

^a Value at reference radius of 1275 km.

the times corresponding to the central-flash data that was excluded from the global fit, the model is not shown in the figure.

The clear upper atmosphere portion of the EY92 model was assumed to be isothermal, see Table 2 and Fig. 2. The data was not of sufficient quality to fit for a thermal gradient in the upper atmosphere, but a higher SNR stellar occultation recorded 1 year earlier in 2006 (Young et al., 2008) showed a thermal gradient in the upper atmosphere of -0.086 K/km. Given this, we decided to investigate the sensitivity of the fitted parameters to the presence of a slight thermal gradient in the upper atmosphere. By fixing the thermal gradient in the EY92 model fit at the value derived from the 2006-occultation data, we find no significant difference in the solutions. As in Young et al. (2008), the f_0 and g_0 offsets (Table 2) are the shift of the shadow location in RA and Dec compared to the shadow location based on the star center and Pluto ephemeris. For this event, the shadow was shifted ~ 500 km east and ~ 884 km south from the position expected from the star position and Pluto ephemeris alone. Note that there is no significant difference in the geometric solution given by the two different fits. While the isothermal and non-isothermal fits have different temperatures and pressures at the reference radius of 1275 km, this is because of the thermal gradient in one model but not in the other. The SNR of the occultation light curve is not sufficient to fit for the thermal gradient so we cannot discriminate between these models. Both solutions have the same half-light radius 1220 km, as expected. Both fits also have a pressure scale height of 55 km. The model light curves are shown in Fig. 3 and the fitted parameters are given in Table 2. The two models (isothermal or assuming a -0.086 K/km gradient) are almost indistinguishable from each other.

We used the EY92 model to derive the parameters that describe Pluto's upper atmosphere and geometric solution (f_0 and g_0). This model also fits the near zero-flux region of light curves with a haze model, but this is not the only interpretation of the light curve data below the radius of 1236 km for these data. The other solution is a thermal gradient and will be addressed later in this paper when we model the central flash.

Given the number and quality of the occultation chords observed for this event, we were unable to fit an elliptical model

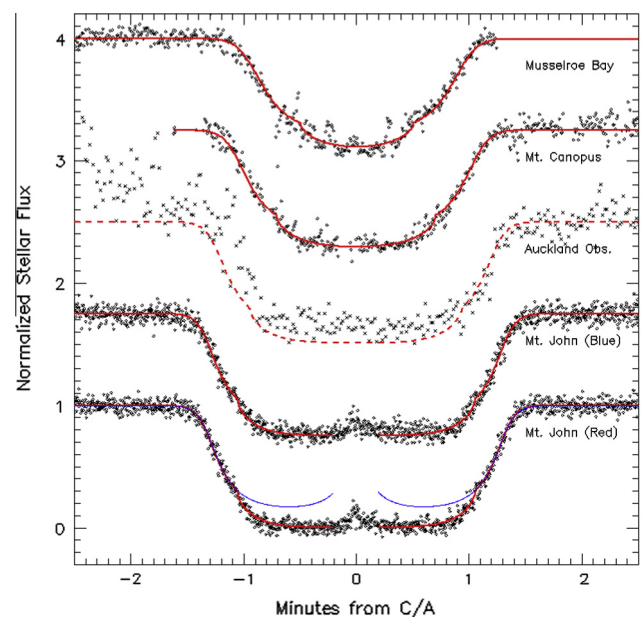


Fig. 3. This figure is the same as Fig. 2 with the exception of the model includes a thermal gradient in the upper atmosphere of -0.086 K/km as derived from the stellar occultation of 2006. There are no significant differences in the two models used to derive the geometric solution.

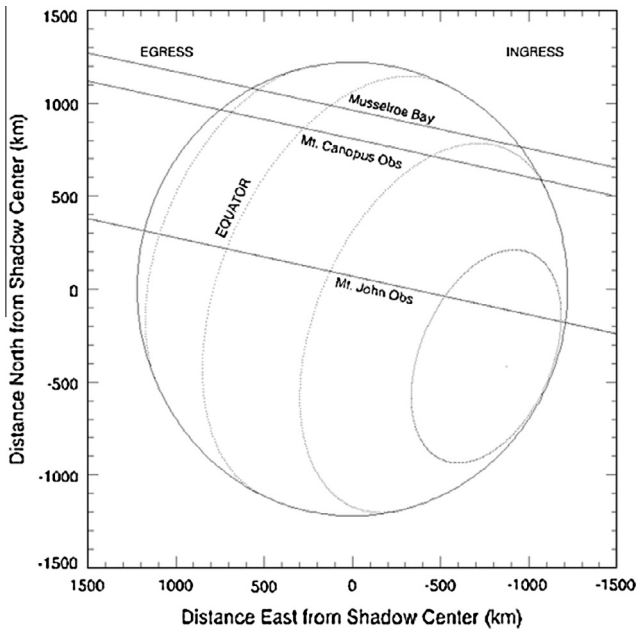


Fig. 4. Pluto's globe as seen from Earth at the time of the occultation. The occultation chords from the three sites are shown. In the figure, North on the sky is up and East is to the right.

for the profile of Pluto's atmosphere. Fig. 4 shows the globe of Pluto as seen from Earth with the occultation chords projected on it.

4. Central flash modeling

A central flash is an increase of observed flux from the occulted star near the center of the shadow due to the focusing of starlight from different locations on the planetary limb. For an atmosphere with an elliptical profile, flux from 4 points on the limb contributes to the central flash. The maximum flux is seen along the evolute of the ellipse (Elliot and Olkin, 1996).

We adapted the method of French et al. (1998) to model the central flash for a small body. The French et al. model was developed to fit central flash observations of Neptune and include the 4 stellar images inside the evolute of the central flash and two stellar images outside this region. We added a term for the partial focusing of the starlight due to the curvature of the planetary limb (see EY92). We modeled the central-flash to derive the shape of Pluto's lower atmosphere and investigate the haze versus thermal-gradient hypotheses for the structure of Pluto's lower atmosphere.

The shape of the central flash light curve depends on the ellipticity of the atmospheric profile and the rotation angle of the ellipse. As the ellipticity of the atmosphere increases the two peaks of the central flash become further apart because the evolute is increasing in size. Fig. 5 shows three central flash light curves corresponding to an atmospheric profile with an ellipticity of 0.06, 0.08 and 0.10. Each of these light curves has the same geometric solution as the Mt. John Observatory observations. The low ellipticity solution intersects the evolute near its edge resulting in a narrow central flash.

The effect rotation angle has on central flash shape is demonstrated in Fig. 6. Different rotation angles will probe the evolute differently resulting in very different central flash light curves. The rotation angle is diagnostic of which peak in the central flash is larger. As seen in the figure, the earlier central flash peak being larger is indicative of a more prolate solution (position angle of the semi-major axis of the ellipse near 90°) rather than an oblate

solution (position angle of the semi-major axis of the ellipse near 0°).

The shape and location of the central flash is diagnostic of the elliptical profile of the atmosphere. The flux level observed in the central flash is indicative of the extinction or thermal gradient in the lower atmosphere. To model the central flash, we started with a model for the isothermal clear upper atmosphere of Pluto based on the fits to all four light curves ('isothermal' column of Table 2). To model the lowest part of the atmosphere probed by the occultation resulting in the observed central flash, we used two different atmospheric models: (i) a haze layer and (ii) a thermal inversion layer. Due to the large bending angle at the center of the light curve, the flux near the central-flash region is only probing a small altitude range on Pluto (less than 1 km). With the rays probing only a small altitude range, we modeled the haze layer with a single optical depth as opposed to the haze scale height model of EY92.

Using the haze model for the atmosphere, we fit for the optical depth and found the optical depth for the blue light curve from Mt. John to be 2.6 ± 1.5 and the ratio of extinction (blue channel to red channel) to be 0.99 ± 0.17 . Note that both channels show similar central flash profiles (Fig. 7) and have similar optical depths. We use this information to constrain the particle sizes. If the particles were much smaller than the wavelength, then we would expect the extinction to go as wavelength to the -4 power which would amount to a factor of 4.9 difference in extinction between the two colors observed. We do not see this large difference in extinction.

We considered scatterers that are approximately the same size as the wavelength to infer the particle size of potential haze particles. Using Mie theory and assuming the haze is composed of tholins (following Elliot et al., 2003), we can model the ratio of the extinctions, see Fig. 8. From our fitted optical depths, we have ratio of the observed extinctions, blue to red, of 1.00 ± 0.22 . From this, we derive a 3-sigma lower-limit on the particle size of $0.2 \mu\text{m}$. Our lower-limit on the particle size is marginally consistent with the haze particle size found in (Elliot et al., 2003) and may indicate that haze particles, if present, have a larger characteristic size than in 2002.

The haze layer considered to match the central flash data is not consistent with the haze in the EY92 modeling of the main drop and recovery of the light curves. The fitting of the EY92 model parameters gives a haze scale height of ~ 2 km below a radius of 1236 km. Extrapolating the haze in the EY92 model from its onset down to a radius of 1130 km with a scale height of 2 km (~ 53 scales heights), we would find significantly more extinction at the central-flash region than we observed. Therefore, if haze is causing extinction of the central-flash rays, we propose it is a detached haze layer – a haze layer that is distinct and lower from the haze layer fit by the EY92 models which is used to explain the “kink” or change of slope of the occultation light curves near a Pluto radius of 1236 km (just below half-light in the light curves). As shown above, the extinction at the central-flash probing altitudes cannot be the same haze layer as the haze used to explain the change in slope during the main drop and recovery of the occultation light curves because its optical depth would be so large at the central-flash probing altitudes as to completely obscure the central flash.

Considering the detached haze layer case, we investigate the location of the central ray, the light that is observed at the midtime of the occultation. This ray would be probing the deepest region of Pluto's atmosphere. For the geometry of this event, the central ray as seen from Mt. John is probing Pluto at a radius of 1130 km. This is significantly smaller than current estimates of Pluto's radius from mutual events 1151–1178 (Tholen and Buie, 1997) or from analysis of high-resolution spectroscopy and occultation of 1169–1172 (Lellouch et al., 2009). Because the detached haze layer

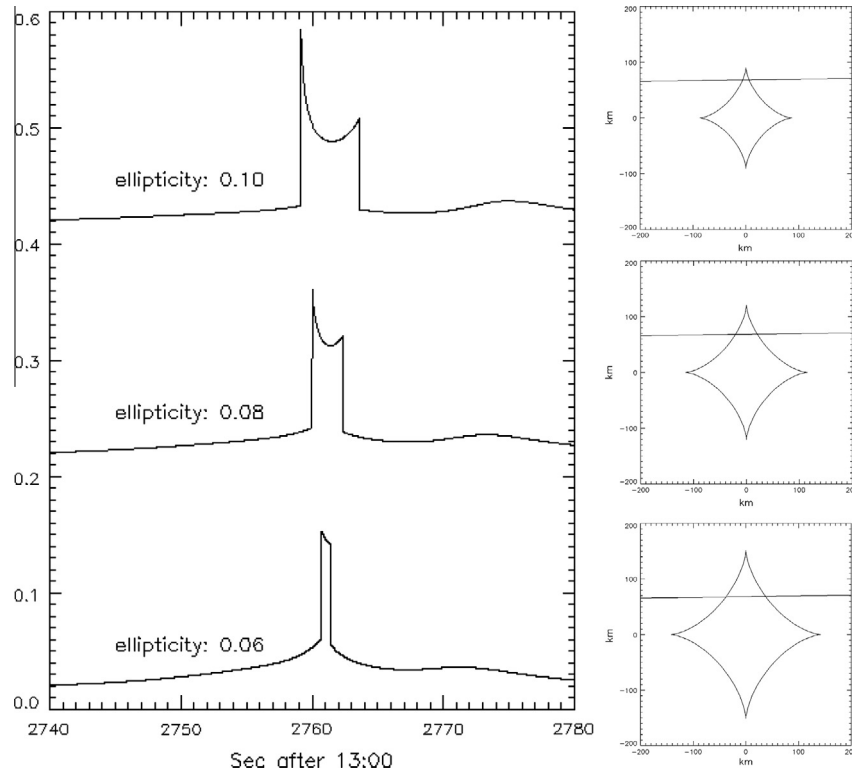


Fig. 5. The effect of different ellipticities on the central flash. The central-flash light curves for 3 different ellipticities from 0.06° , 0.08° and 0.1° are shown on the left. The right panel shows the relative path of the star as seen from the Mt. John Observatory through the evolute. The position angle of the ellipticity is 90° for these figures.

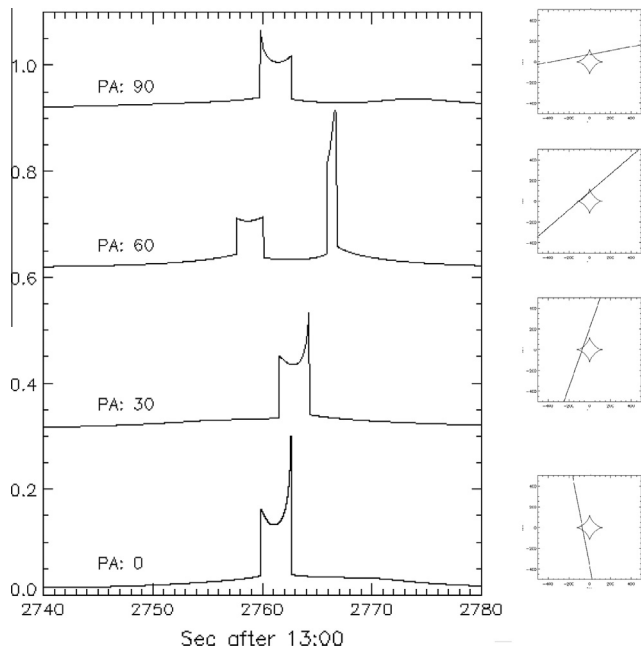


Fig. 6. The effect of different position angles (PA) on the central flash. The central-flash light curves for 4 different position angles from 0° to 90° are shown on the left. The right panel shows the relative path of the star through the evolute for a closest approach distance between the star and the planet equal to the Mt. John Observations.

explanation requires an unrealistically small radius of Pluto (<1130 km), we do not adopt this as our solution.

Next we consider a purely refractive lower atmosphere to model the central flash. A thermal gradient of 5 K/km can

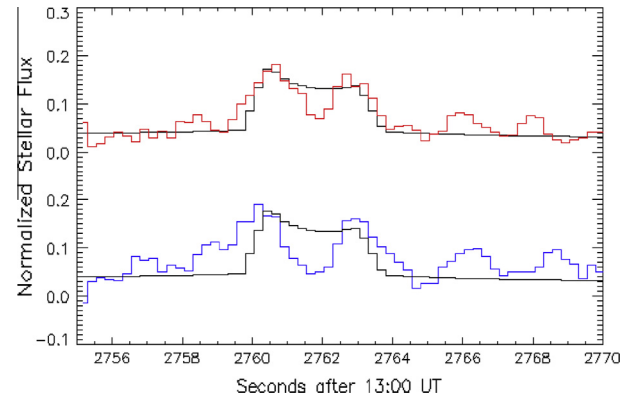


Fig. 7. The central flash data (red and blue; binned by 2) and the light curve model at the same resolution based on an elliptical atmospheric profile and haze in the lower atmosphere to match the observed flux of the central peaks. The ellipticity of the atmosphere is 0.09 and the orientation of the major axis of the ellipse is 100° from the equatorial plane. The optical depth for the blue filter is 2.5 ± 1.6 (blue) and the ratio of the extinction (blue to red) is 1.00 ± 0.22 . The uncertainty in the flux level at the central flash is 0.03 in units of normalized stellar flux. (For interpretation of the references to color in this figure legend, the reader is referred to the web version of this article.)

reproduce the central-flash data as seen in Fig. 9. The rays in this purely refractive case experience more bending than the extinction only case previously examined. These rays would probe Pluto's atmosphere down to a radius of 1196 km – a radius that is plausible given estimates of Pluto's size. It could be that Pluto's lower atmosphere is composed of some extinction and some thermal gradients. We considered only the end members. Modeling the intermediate states (combinations of thermal gradients and extinction) would be an area of future work.

For our elliptical atmospheric model both the purely extinction and purely refractive models, the best solution is a nearly prolate

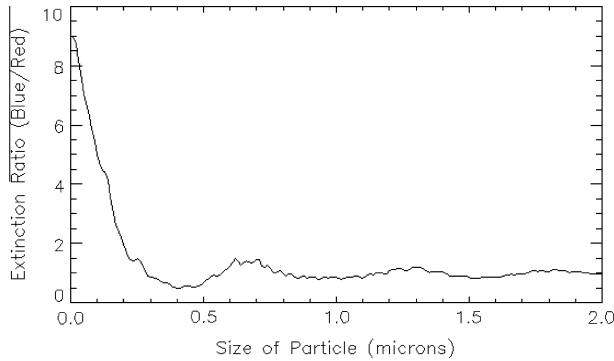


Fig. 8. Ratio of extinction in the blue channel relative to the red channel as a function of particle size. We have assumed Triton tholin particles.

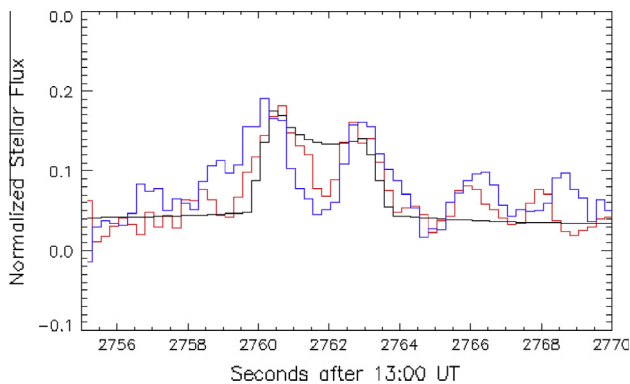


Fig. 9. The central flash data (red and blue; binned by 2) and the light curve model (at the same resolution) based on a prolate atmosphere and a thermal gradient. The ellipticity of the atmosphere is 0.09 and the orientation of the major axis of the ellipse is 100° from the equatorial plane. The thermal gradient is 3.5 K/km. The uncertainty in the flux level at the central flash is 0.03 in units of normalized stellar flux. (For interpretation of the references to color in this figure legend, the reader is referred to the web version of this article.)

spheroid shape (angle to the equator of 100°) with an ellipticity of 0.09. A prolate solution is favored slightly because the double peak of the central flash shows a higher initial peak. The significance of the height difference between the first and second peak is 1.0 sigma for the light curve recorded with the blue channel and 1.22 sigma for the light curve in the red channel. An oblate atmosphere model for the geometry of the solution would have the second peak higher than the first, as shown in Fig. 6. This is why the prolate solution fits better than the oblate solution. We acknowledge that we do not have physical explanations of the prolate solution. This is likely a result of our simplified elliptical model. With variable hazes or thermal gradients around Pluto's limb the contribution of each stellar image contributing to the evolute could sample a different environment and this is not included in our model. Longitudinal varying thermal gradients or intermittent hazes could sculpt the central flash model to better fit the data in between the central flash peaks. Also, one could imagine the contribution of one stellar image composing the signal at the evolute being reduced due to haze and this could make an oblate atmosphere appear like a prolate atmosphere by reducing the flux at the secondary central peak.

Person (2006) used two multi-chord Pluto occultations to determine the shape of Pluto's atmosphere. He analyzed both the 1988 and 2002 stellar occultation (with six sites observing the event) to derive an elliptical model for the profile of Pluto's atmosphere. For

both events, he was fitting for the shape of the atmosphere at a much higher altitude than the central flash measures. For the 2002 event, he used the times that the light curves measured 94% of the normalized stellar flux and for the 1988 event, he used the 74% normalized stellar flux level. In both cases, these flux levels were chosen because some chords did not probe below these levels. His fitted ellipticities (0.091 ± 0.041 and 0.066 ± 0.044) are similar to our finding, but the orientation of the ellipse is consistent with an oblate solution for 2002 and about 25° from oblate for the 1988 data, whereas, these results are consistent with an orientation that is within 5° of prolate.

These different solutions are investigating the shape of the atmosphere at two very different altitudes (more than ~ 100 km different) and using two different techniques. In Person (2006) they are using lines of constant stellar flux to infer an isopycnal surface. In this work, we are using the 4 stellar images that contribute to the evolute as they travel along Pluto's limb to derive a surface of equal bending angle. With a Pluto Global Circulation Model (GCM), we could improve our interpretation of Pluto's atmosphere by using a more sophisticated model for the planetary atmosphere and model the resulting central flash. Our model to date does not accommodate longitudinally constrained hazes or thermal gradients that are different from one location to the next. This type of variability is the next step in modeling the central flash and will allow us to model the minimum between the central flash peaks more accurately.

5. Conclusions

We observed a stellar occultation by Pluto from four sites in July 2007 including the first central flash of Pluto. The stellar occultation light curves show that the atmospheric pressure on Pluto ($2.09 \mu\text{bar}$ from our non-isothermal solution) is increasing slightly over the previous measurement in 2006 ($1.86 \mu\text{bar}$ from Young et al., 2008) and is still more than double the value in 1988 ($0.83 \mu\text{bar}$ from Elliot and Young, 1992). For consistency of comparison, all of these values were fit to the non-isothermal EY92 atmospheric model. The atmosphere has not yet begun to collapse as Pluto recedes from the Sun.

From the nearly central chord observed at Mt. John Observatory, we see a central-flash occultation. This occultation is well modeled by a prolate atmosphere with an ellipticity of 0.09 although a more sophisticated model with longitudinally variable hazes or thermal gradients might find a solution that is consistent with an oblate atmosphere. The modeling results exclude a haze only mechanism to match the central-flash flux because the light contributing to the central flash would be coming from below the surface of Pluto for current best estimates of Pluto's size. A clear atmosphere with a thermal gradient of 5 K/km at a radius of 1196 km matches the central-flash data.

Acknowledgments

We thank Martin George and Chris Arkless of the Queen Victoria Museum and Gallery, for logistical support in Tasmania. Chris Arkless kindly loaned us the use of his cottage at Musselroe Bay providing a clear site for our portable telescope. We also thank Simon McCulloch and Andrew McGifford at the Bureau of Meteorology in Launceston Tasmania for their expertise in weather predictions. We would also like to thank Alan Gilmore and the staff at Mt. John Observatory for their assistance. This work was supported by NASA Planetary Astronomy Grant NNG05GF05G and NSF Major Research Instrumentation Grant AST0321338.

References

- Cruikshank, D.P., Pilcher, C.B., Morrison, D., 1976. Pluto – Evidence for methane frost. *Science* 194, 835–837.
- Elliot, J.L., Olkin, C.B., 1996. Probing planetary atmospheres with stellar occultations. *Annu. Rev. Earth Planet. Sci.* 24, 89–124.
- Elliot, J.L., Young, L.A., 1992. Analysis of stellar occultation data for planetary atmospheres. I. Model fitting, with application to Pluto. *Astron. J.* 103, 991–1015.
- Elliot, J.L., Dunham, E.W., Bosh, A.S., Slivan, S.M., Young, L.A., Wasserman, L.H., Millis, R.L., 1989. Pluto's atmosphere. *Icarus* 77, 148–170.
- Elliot, J.L. et al., 2003. The recent expansion of Pluto's atmosphere. *Nature* 424, 165–168.
- French, R.G., McGhee, C.A., Sicardy, B., 1998. Neptune's stratospheric winds from three central flash occultations. *Icarus* 136, 27–49.
- Greaves, J.S., Helling, Ch., Friberg, P., 2011. Discovery of carbon monoxide in the upper atmosphere of Pluto. *Mon. Not. R. Astron. Soc.* 247–252, L36–L40.
- Hansen, C.J., Paige, D.A., 1996. Seasonal nitrogen cycles on Pluto. *Icarus* 120, 247–265.
- Lellouch, E., Sicardy, B., de Bergh, C., Kaufl, H.-U., Kassi, S., Campargue, A., 2009. Pluto's lower atmosphere structure and methane abundance from high-resolution spectroscopy and stellar occultations. *Astron. Astrophys.* 495, L17–L21.
- Lellouch, E., de Bergh, C., Sicardy, B., Kaufl, H.U., Smette, A., 2011. High resolution spectroscopy of Pluto's atmosphere: Detection of the 2.3 mm CH₄ bands and evidence for carbon monoxide. *Astron. Astrophys.* 530, L1–L4.
- McDonald, S.W., Elliot, J.L., 2000. Pluto–Charon stellar occultation candidates: 2000–2009. *Astron. J.* 119, 1999–2007.
- Owen et al., 1993. Surface ices and the atmospheric composition of Pluto. *Science* 261, 745–748.
- Person, M.J., 2006. The Use of Stellar Occultations to Study the Figures and Atmospheres of Small Bodies in the Outer Solar System. MIT Ph.D. Thesis.
- Sicardy, B. et al., 2003. Large changes in Pluto's atmosphere as revealed by recent stellar occultations. *Nature* 424, 168–170.
- Tholen, D.J., Buie, M.W., 1997. Bulk properties of Pluto and Charon. In: Stern, S.A., Tholen, D.J. (Eds.), *Pluto and Charon*. The University of Arizona Press.
- Young, L.A., 2013. Pluto's seasons: New predictions for New Horizons. *Astrophys. J.* 766, L22–L28.
- Young, L.A., Elliot, J.L., Tokunaga, A., de Bergh, C., Owen, T., 1997. Detection of gaseous methane on Pluto. *Icarus* 127, 258–262.
- Young, E.Y. et al., 2008. Vertical structure in Pluto's atmosphere from the 2006 June 12 stellar occultation. *Astron. J.* 136, 1757–1769.
- Young, E.F. et al., 2011. Development and performance of the PHOT (Portable High-Speed Occultation Telescope) systems. *Publ. Astron. Soc. Pacific* 123, 735–745.
- Zacharias et al., 2004. The second US naval observatory CCD astrograph catalog (UCAC2). *Astron. J.* 127, 3043–3059.